Bioactive Materials 29 (2023) 251–264

Contents lists available at ScienceDirect

Bioactive Materials

journal homepage: www.keaipublishing.com/en/journals/bioactive-materials

Macrophage metabolism reprogramming EGCG-Cu coordination capsules delivered in polyzwitterionic hydrogel for burn wound healing and regeneration

Qinghua Li [a,1], Huijuan Song [b,1], Shuangyang Li [c], Pengbo Hu [d], Chuangnian Zhang [a], Ju Zhang [a], Zujian Feng [a,***], Deling Kong [e], Weiwei Wang [a,*], Pingsheng Huang [a,**]

[a] Tianjin Key Laboratory of Biomaterial Research, Institute of Biomedical Engineering, Chinese Academy of Medical Sciences and Peking Union Medical College, Tianjin, 300192, China
[b] Institute of Radiation Medicine, Chinese Academy of Medical Sciences and Peking Union Medical College, Tianjin, 300192, China
[c] Department of Polymer Science and Engineering, Key Laboratory of Systems Bioengineering, School of Chemical Engineering and Technology, Tianjin University, Tianjin, 300072, China
[d] Emergency Department of Binzhou Medical University Hospital, Binzhou, Shandong Province, 256600, China
[e] State Key Laboratory of Medicinal Chemical Biology, College of Life Sciences, Nankai University, Tianjin, 300071, China

ARTICLE INFO

Keywords:
ROS scavenging
Hydrogel dressing
EGCG-Cu capsule
Metabolic reprogramming
Burn wound healing

ABSTRACT

Excessive reactive oxygen species (ROS) at severe burn injury sites may promote metabolic reprogramming of macrophages to induce a deteriorative and uncontrolled inflammation cycle, leading to delayed wound healing and regeneration. Here, a novel bioactive, anti-fouling, flexible polyzwitterionic hydrogel encapsulated with epigallocatechin gallate (EGCG)-copper (Cu) capsules (termed as EGCG-Cu@CB^{gel}) is engineered for burn wound management, which is dedicated to synergistically exerting ROS-scavenging, immune metabolic regulation and pro-angiogenic effects. EGCG-Cu@CB^{gel} can scavenge ROS to normalize intracellular redox homeostasis, effectively relieving oxidative damages and blocking proinflammatory signal transduction. Importantly, EGCG-Cu can inhibit the activity of hexokinase and phosphofructokinase, alleviate accumulation of pyruvate and convert it to acetyl coenzyme A (CoA), whereby inhibits glycolysis and normalizes tricarboxylic acid (TCA) cycle. Additionally, metabolic reprogramming of macrophages by EGCG-Cu downregulates M1-type polarization and the expression of proinflammatory cytokines both *in vitro* and *in vivo*. Meanwhile, copper ions (Cu^{2+}) released from the hydrogel facilitate angiogenesis. EGCG-Cu@CB^{gel} significantly accelerates the healing of severe burn wound *via* promoting wound closure, weakening tissue-damaging inflammatory responses and enhancing the remodeling of pathological structure. Overall, this study demonstrates the great potential of bioactive hydrogel dressing in treating burn wounds without unnecessary secondary damage to newly formed skin, and highlights the importance of immunometabolism modulation in tissue repair and regeneration.

1. Introduction

Burn injuries, particularly severe burns, are the most traumatic and physically debilitating cutaneous injuries, which can affect nearly every organ and cause substantial morbidity and mortality worldwide [1,2]. Skin grafting remains the gold standard for treating severe burn wounds in clinic, which can reduce the mortality rate and duration of patient hospitalization [3,4]. However, drawbacks including limited donor skin, fragility, rough texture, and increased scar contractures, limit the autologous skin grafting in practice [5,6]. Moreover, the chronic wound healing process caused by repeated bacteria infection and persistent inflammatory response can lead to hypertrophic scarring, ulceration and

Peer review under responsibility of KeAi Communications Co., Ltd.
* Corresponding author.
** Corresponding author.
*** Corresponding author.
E-mail addresses: fzujian@163.com (Z. Feng), wwangtj@163.com (W. Wang), sheng1989.2008@163.com (P. Huang).
[1] These authors contributed equally to this work.

https://doi.org/10.1016/j.bioactmat.2023.07.011
Received 9 February 2023; Received in revised form 30 June 2023; Accepted 13 July 2023

even amputation, and thus remains a major challenge in burn management [7]. Therefore, modulating the inflammatory response is an important therapeutic strategy in managing wound healing with the aim of disrupting the chronic inflammation. Hydrogel dressings have recently received tremendous interest owing to their considerable advantages, including absorption of wound exudate and maintenance of a moist environment and skin adaptiveness [8,9]. In particular, hydrogels can be engineered as a platform with various biological functions to regulate the inflammatory microenvironment by delivering drugs or cytokines, scavenging the proinflammatory mediators, and providing biochemical cues for immune cell modulation [10–12]. However, current immunomodulatory approaches in developing bioactive hydrogel dressings do not pay sufficient attention to the complexity of the multi-cellular response and the special pathology characters during burn wound healing and regeneration.

Poor healing in burn wounds is often associated with immune dysfunction leading to severe tissue destruction and extensive inflammatory reactions with a spectrum of pathological phases [13]. Upon injury, pro-inflammatory cells, including macrophages and neutrophils, infiltrate and induce the release of multiple inflammatory mediators, such as interleukin (IL)-1, IL-6, IL-8, IL-18, tumor necrosis factor-α (TNF-α), and reactive oxygen species (ROS) [14–17]. In particular, ROS directly induce cell apoptosis because of the lethal oxidative damage to DNA, proteins and lipid peroxidation of membranes, which is implicated in tissue damage and even multiple organ failure [13,18]. In addition, ROS are closely related with local and systemic inflammatory reactions, and acts as key signaling molecules to affect the recruitment and function of inflammatory cells [19–21]. Specifically, ROS accumulation in wound sites primes the macrophages into the pro-inflammatory M1 phenotype through structural dysfunction of macrophage mitochondria and promoting the glycolysis [22], which is known to be the core driving force for initiating the inflammatory response. The enhanced glycolytic metabolism of M1-type macrophages impairs the tricarboxylic acid (TCA) cycle and mitochondrial oxidative phosphorylation (OXPHOS), and thus stabilizes hypoxia-inducible factor 1 (HIF-1α) protein, down-regulating succinate dehydrogenase (SDH) [23–25]. Massive accumulation of succinate regulates the mitochondrial transition from ATP synthesis to mitochondrial-derived ROS production [26], and the amplification of ROS at the wound site further recruits macrophages and polarizes them into M1 type, thus initiating an uncontrolled inflammation cycle and delayed wound healing. Accordingly, we hypothesized that effective ROS scavenging and reprogramming the glycolytic metabolism in macrophage might alleviate oxidative stress damage and inhibit the cycle of inflammation, thereby accelerating the healing of severe burns.

Herein, we proposed a bioactive hydrogel platform for burn wound care with the encapsulation of an epigallocatechin gallate (EGCG)-copper (Cu) metal organic framework capsule (Fig. 1), which was expected to integrate synergistical effects of ROS-scavenging, immune metabolic regulation, and pro-angiogenesis. EGCG, one of the most abundant polyphenols in tea, has several biological effects, including anti-bacteria, anti-inflammation, and anti-oxidation [27–30]. In particular, EGCG regulates the phenotypic changes and metabolic reprogramming of macrophages by interfering with glycolysis [31,32]. Additionally, copper ions (Cu^{2+}) can promote angiogenesis by inducing the secretion of vascular endothelial growth factor (VEGF) [33–35], and stabilize EGCG by forming chelate complex to improve its bioavailability [36]. Therefore, a metal-polyphenol capsule (EGCG-Cu) was developed by the formation of an EGCG-Cu coordination network to sustainably release EGCG and Cu^{2+} at the injury site, enabling the hydrogel to modulate the inflammatory microenvironment and pro-angiogenesis. Moreover, the zwitterionic hydrogel with anti-adhesion properties and flexible mechanics was applied as a wound dressing, which could not only retain bioactive EGCG-Cu capsules in the wound bed, but also prevent bacterial adhesion and unnecessary secondary damages to the newly formed skin tissue. Using these unique advantages, this work demonstrated that

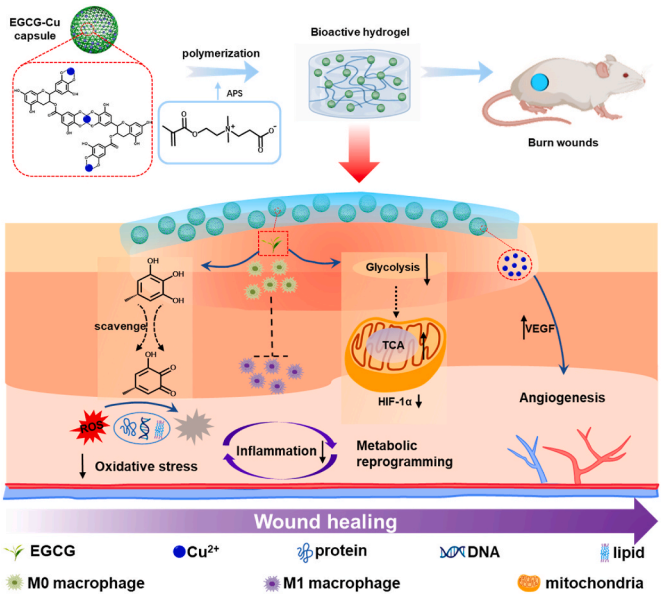

Fig. 1. Bioactive EGCG-Cu@CB^{gel} for severe burn wound healing *via* ROS scavenging, metabolic reprogramming of macrophages, and pro-angiogenesis. EGCG-Cu@CB^{gel} was prepared *via* one-pot free radical copolymerization of carboxybetaine monomer (CB) and the zwitterionic crosslinking agent (termed as CBOX), while EGCG-Cu capsules were loaded during the polymerization process. EGCG released from the hydrogels could scavenge excess ROS to reduce oxidative stress damage and regulate the glycolysis of macrophages, collaboratively inhibiting inflammation *via* TCA cycling. Cu^{2+} promoted the secretion of VEGF for angiogenesis. Thus, EGCG-Cu capsules-delivering polyzwitterionic hydrogel accelerated the regenerative burn wound healing.

EGCG-Cu capsule-encapsulated hydrogel dressing could greatly accelerate the burn wound healing and angiogenesis through the scavenging of toxic ROS together with regulating TCA cycle in macrophages, providing an effective strategy for chronic wound management.

2. Materials and methods

Materials including chemical regents and antibodies used in this study are shown in supporting information file.

Synthesis of EGCG-Cu capsules: $CaCO_3$ particles were first synthesized *via* a rapid co-precipitation method. Briefly, poly (sodium 4-styrenesulfonate) (PSS, 20 mg) was completely dissolved in $CaCl_2{\cdot}2H_2O$ solution (0.33 M, 10 mL), and then quickly poured into Na_2CO_3 (0.33 M, 10 mL) and stirred continuously for 30 s. The precipitate was centrifuged (3000 rpm, 2 min) and washed thrice with deionized water. Subsequently, EGCG (24 mM, 4 mL), $CuCl_2{\cdot}2H_2O$ (24 mM, 4 mL), and 3-morpholinopropanesulfonic acid solutions (MOPS, 100 mM, pH 8.0, 4 mL) were sequentially added to the $CaCO_3$ precipitate with vortex for 60 s. The mixture was then centrifuged (3000 rpm, 2 min) and washed with deionized water and repeated thrice. Finally, ethylene diamine tetraacetic acid (EDTA) solution (100 mM, pH 8.0, 10 mL) was added to the precipitate and shaken for 10 min to dissolve the $CaCO_3$ template, and the product was obtained by washing twice. The surface morphology was investigated using scanning electron microscope (SEM; S-4800, Hitachi, Japan). The binding energy were detected using X-ray photoelectron spectroscopy (XPS; Thermo, ESCALAB XI, USA). Fourier transform infrared spectrometer (FTIR; Thermo, NICOLET iS10, Finland) was used to analyze the major functional groups of EGCG- Cu capsules.

Synthesis of EGCG-Cu@CB^{gel}: Carboxybetaine zwitterionic hydrogels (termed as CB^{gel}) were prepared *via* free radical copolymerization of carboxybetaine monomer (CB) and 1-carboxy-N-methyl-N-di(2-methacryloyloxy-ethyl) methanaminium inner salt crosslinking agent

(termed as CBOX). CB monomer was dissolved in deionized water at a concentration of 30 wt% and CBOX was added to the monomer solution at 2 wt% (% of CB). After degassing, pre-dissolved thermal initiator ammonium persulfate (APS) and EGCG-Cu capsules (0.02 wt% of deionized water) were added to the above solution, and the obtained solution was incubated at 60 °C for 4 h to obtain EGCG-Cu@CB^{gel}.

In vitro Cu ions release: The release of Cu^{2+} from EGCG-Cu@CB^{gel} was assessed in phosphate-buffered saline (PBS, pH 7.4) with or without H_2O_2 at 37 °C. Briefly, EGCG-Cu@CB^{gel} samples were incubated in 5 mL PBS or H_2O_2 (40 μM) with continuous shaking (100 rpm). At predetermined time intervals, release medium (1 mL) was extracted and an equal amount of fresh medium was supplemented. The amount of released Cu was measured using inductively coupled plasma mass spectrometry (ICP-MASS; PerkinElmer, NexION 300X, USA).

In vitro ROS scavenging activity: The H_2O_2 scavenging abilities of EGCG-Cu capsules were assessed at 25 °C. A volume of 50 μL of H_2O_2 solution (40 μM (PBS, 25 mM, pH 7.4) was added into individual wells of a 96-well microplate, and then 50 μL of EGCG-Cu capsules at different concentrations were added. After reaction for 2 h, the H_2O_2 concentration was measured by Amplite™ Hydrogen Peroxide Assay Kit according to the manufacturer's protocol (AAT Bioquest, USA).

2,2-Diphenyl-1-picrylhydrazyl (DPPH) free radical scavenging by EGCG-Cu capsules was further evaluated according to a previously described radical scavenging assay [10]. Briefly, different concentrations of EGCG-Cu suspension were added into 2 mL of DPPH ethanol solution (100 μM) and ethanol was used as control. After incubating for 30 min, the absorbance of the supernatants was measured at 513 nm with a Varioskan Flash Microplate Reader (Thermo Fisher Scientific).

Intracellular ROS scavenging activity and antioxidation: Antioxidant analysis of EGCG-Cu capsules (25 μg mL^{-1}) was conducted against HUVEC cells. HUVEC cells were seeded in 96-well plates at a density of 1×10^4 cells per well. Fresh media (100 μL) containing EGCG-Cu capsules (10 μL) were added. Cells were stimulated with H_2O_2 (100 μM) to produce excess ROS. The cell viability was then evaluated with a cell counting kit-8 (CCK-8) assay.

To study the scavenging ability of EGCG-Cu capsules of intracellular ROS, HUVEC cells at a density of 2×10^4 cells per well were seeded in a 24-well plate and pre-treated with Rosup (100 μg mL^{-1}) to elevate the intracellular ROS level for 4 h. Dichlorodihydrofluorescein diacetate (DCFH-DA) was employed to detect the intracellular ROS level.

Mitochondrial function and metabolism of macrophages: RAW 264.7 cells were seeded in 6-well plates at a density of 1×10^5 cells per well and stimulated with lipopolysaccharide (LPS) for 24 h. Cells were then incubated with EGCG-Cu capsules for 24 h to investigate the level of mitochondrial membrane potential (MMP) and adenosine triphosphate (ATP).

The MMP values were determined using the JC-1 MMP Assay Kit (Beyotime Biotechnology). Briefly, cells were washed twice and then incubated with JC-1 staining working solution for 20 min. Subsequently, the cells were washed twice with JC-1 dilution buffer and immediately observed using laser confocal scanning microscope (CLMS). Flow cytometry was performed to detect the fluorescence intensity. For ATP determination, cells were first washed and lysed at 4 °C, and lysed cells were centrifuged at 12000 g, and the supernatant (20 μL per well) was added to a black 96-well plate (Thermo Scientific, Madison, WI, USA) containing ATP working solution (100 μL per well). Luminescence values of resulted solutions were measured using an enzyme marker (Infinite M200 Pro, Tecan, Switzerland). The activities of hexokinase (HK) and phosphofructokinase (PFK) were measured by Hexokinase Activity Assay Kit (AKSU061 M) and Phosphofructokinase Activity Assay Kit (AKSU062 M) according to the manufacturer's manual (Boxbio Science & Technology Co., Ltd., Beijing, China).

To investigate the effect of EGCG-Cu capsules on cell metabolism, RAW 264.7 cells were inoculated in 60 mm culture dishes and pre-stimulated with LPS for 24 h. Cells were then incubated with EGCG-Cu capsules for another 24 h. Subsequently, cells were collected and ground in liquid nitrogen. Prechilled methanol/acetonitrile/water (2:2:1, v/v/v; 1 mL) was added to each sample and sonicated for 30 min in an ice bath and repeated twice. Proteins were precipitated *via* incubation at −20 °C for 1 h and then centrifuged at 12,000 rpm, and the supernatant was discarded and aspirated for vacuum drying. For mass spectrometry, 200 μL of acetonitrile/water solution (1:1, v/v) was added and analyzed using an instrumentation system equipped with ultra performance liquid chromatography (Vanquish, UPLC, Thermo, USA) and high resolution mass spectrometry (Q Exactive, Thermo, USA) equipped with a Waters BEH Amide column (100 × 2.1 mm, 1.8 μm). Data were processed using the TraceFinder software.

In vitro macrophage polarization: Bone marrow derived macrophages (BMDMs) were isolated from C57BL/6 mice and cultured for 7 days, as previously described [37]. Macrophages were pre-incubated with 100 ng mL^{-1} LPS for 24 h and then incubated with EGCG-Cu. After 48 h, cells were collected *via* centrifugation and washed twice with cold PBS. Treated cells were stained with FITC-labeled anti-CD80 antibodies, PE-labeled F4/80 antibodies and APC-labeled CD206 according to the manufacture's guidelines, and then analyzed *via* flow cytometry (C6, BD, USA). The gene expression of inducible nitric-oxide synthase (iNOS), IL-1β, and CD86 in macrophages was measured *via* quantitative reverse transcription-polymerase chain reaction (qRT-PCR). The expression level of IL-6 and TNF-α in the media was measured with a commercially available ELISA kit (cusabio, Wuhan, China). The expression of NF-κB p65 and HIF-1α was determined *via* western blotting. RIPA lysis buffer (Beyotime, P0013B) containing 1 mM phenylmethanesulfonyl fluoride (PMSF) (Beyotime, ST506) was applied to obtain total cell lysates of treated macrophages.

In vivo burn wound healing model and histological analysis: Burn wound models were established on the backs of BALB/C mice. Before surgery, the mice were anesthetized with isoflurane, and the dorsum was shaved and then wiped with alcohol to disinfect. The bare dorsum of mice was burned using scald apparatus (YLS-5Q) at 100 °C for 10 s. Mice were also injected subcutaneously with meloxicam at a dose of 5 mg kg^{-1} for pain relief. Wound-bearing mice were randomly divided into four groups, including control, CB^{gel}, EGCG-Cu, and EGCG-Cu@CB^{gel}, with 17 mice in each group. Each wound was covered with a sheet of Tegaderm (3 M). Wound areas were recorded at different times with a digital camera and hydrogels were replaced at day 3, 7, and 10. The wound closure rate was calculated by comparing the wound area at sampling time with that at day 0.

On day 3, 7, and 14, wound tissue samples (n = 5) were collected and fixed with 4% formaldehyde, dehydrated, and embedded in paraffin, and then cross-cut into 5 μm thick sections. Tissue slices were stained with hematoxylin and eosin (H&E, G1120, Solarbio Life Science) and Masson's trichrome stain to evaluate the histomorphology of the regenerated skin tissue.

Dihydroethidium (DHE) staining was used to evaluate the ROS scavenging *in vivo*. Tissues isolated at the third day were sliced, and then rewarmed at room temperature. Circles were drawn around the tissues with a histology marker pen, and self-luminous fluorescence quencher was added and incubated for 5 min, followed by a 10-min water rinse. ROS dye solution was added to the circle, which was incubated at 37 °C in dark for 30 min, and washed in a decolorizing shaker for 3 times. Then 4,6-diamidino-2-phenylindole (DAPI) dye solution was added and incubated at room temperature in dark for 10 min and washed in PBS (pH 7.4) for 3 times. Finally, the slices were sealed with anti-fluorescence quenching tablets.

Immunofluorescence staining of tissues was used to evaluate angiogenesis and inflammation. Skin tissue slices were dewaxed and then placed in antigen retrieval buffer for antigen retrieval in a microwave oven. Then, circle autofluorescence quenching was performed on the tissue sections. Tissue slices were washed with PBS and then sealed with goat serum at room temperature for 2 h. The slices were then incubated with rabbit polyclonal antibody against CD31 (1:200, Abcam), mouse polyclonal antibody against α-SMA (1:200, Abcam), mouse polyclonal

antibody against CD68 (1:200, Abcam), and rabbit polyclonal antibody against CD86 (1:200, Bioss), respectively. After incubation overnight in 4 °C, the slices were washed with PBS (pH 7.4) on a shaking bed for 3 times, 5 min each time. After drying, the second antibody corresponding to the primary antibody was added and incubated at room temperature for 1 h. Then the slices were washed with PBS (pH 7.4) on a shaking bed for 3 times, 5 min each time. Finally, DAPI staining solution was incubated at room temperature for 10 min and washed in PBS (pH 7.4) for 3 times. The slices were sealed with anti-fluorescence quenching tablets, and observed with microscope and quantitatively analyzed by ImageJ software.

All animal procedures were performed in accordance with the Guidelines for the Care and Use of Laboratory Animals of Peking Union Medical College and experiments were approved by the Animal Experiments and Ethics Review Committee of the Institute of Radiation Medicine, Chinese Academy of Medical Sciences (No. IRM-DWL-2021043).

Statistical analysis: Statistical analyses were performed with GraphPad Prism software (version 8.0). Statistical significance between two or multiple groups was performed with *t*-test or one-way ANOVA, respectively. Data are presented as mean ± standard deviations (SDs). Statistical significance was denoted by *$p < 0.05$, **$p < 0.01$, or ***$p < 0.001$.

3. Results and discussion

3.1. Synthesis and characterization of EGCG-Cu@CB^{gel}

A zwitterionic hydrogel dressing encapsulated with EGCG-Cu metal organic framework capsules was rationally designed and fabricated. The pyrocatechol structure of EGCG could cooperate with multiple types of metals ions to form a metal organic framework with controllable size and shapes to prolong bioavailability [30]. EGCG has antioxidant ability that can obliterate exvessive ROS and it is found that EGCG-based hydrogel without any metal ions can accelerate diabetic wound healing by decreasing ROS and inducing M2 phenotype polarization [38]. However, as a small molecule, low bioavailability and stability limit its application. Recently, metal-phenol coordination materials have been developed to form complexes, which improve the stability and extend the residence time period *in vivo* [36,39]. Cu was an essential modulator of multiple cellular signaling pathways with a vital role in angiogenesis *via* the regulation of endothelial cell survival, proliferation, and migration [40,41]. At the initiation stage of angiogenesis, Cu activates and amplifies angiogenic responses induced by major pro-angiogenic stimuli, including hypoxia and growth factors such as VEGF and fibroblast growth factor (FGF). During endothelial cell proliferation, migration, and morphogenesis, the specific binding of Cu to angiogenin, a major angiogenic factor, is able to argument the interaction with endothelial cells. During extracellular matrix (ECM) remodeling, Cu acts as a co-factor for members of the LOX (lysine oxidase) enzyme family, catalyzing the crosslinking of collagen and elastin, contributing to the stability of ECM [40,42]. Therefore, EGCG-Cu capsules were fabricated to synergistically enhance angiogenesis through multiple mechanism. Furthermore, Cu existing either in the oxidized or reduced state (Cu^{+} or Cu^{2+}) has inherent redox property, which could maintain redox homeostasis by serving as a cofactor for oxidase and antioxidant enzymes, including lysyl oxidase, Cu/Zn superoxide dismutase (SOD), retina-specific amine oxidase, etc. [43] Hence, EGCG-Cu capsules were also expected to increase the antioxidant activity of EGCG. As shown in Fig. 2A, EGCG-Cu capsules were prepared *via* the co-precipitation method. The aqueous solutions of EGCG and $CuCl_2$ were deposited onto $CaCO_3$ particles, which was followed by removal of $CaCO_3$ templates with EDTA solution.

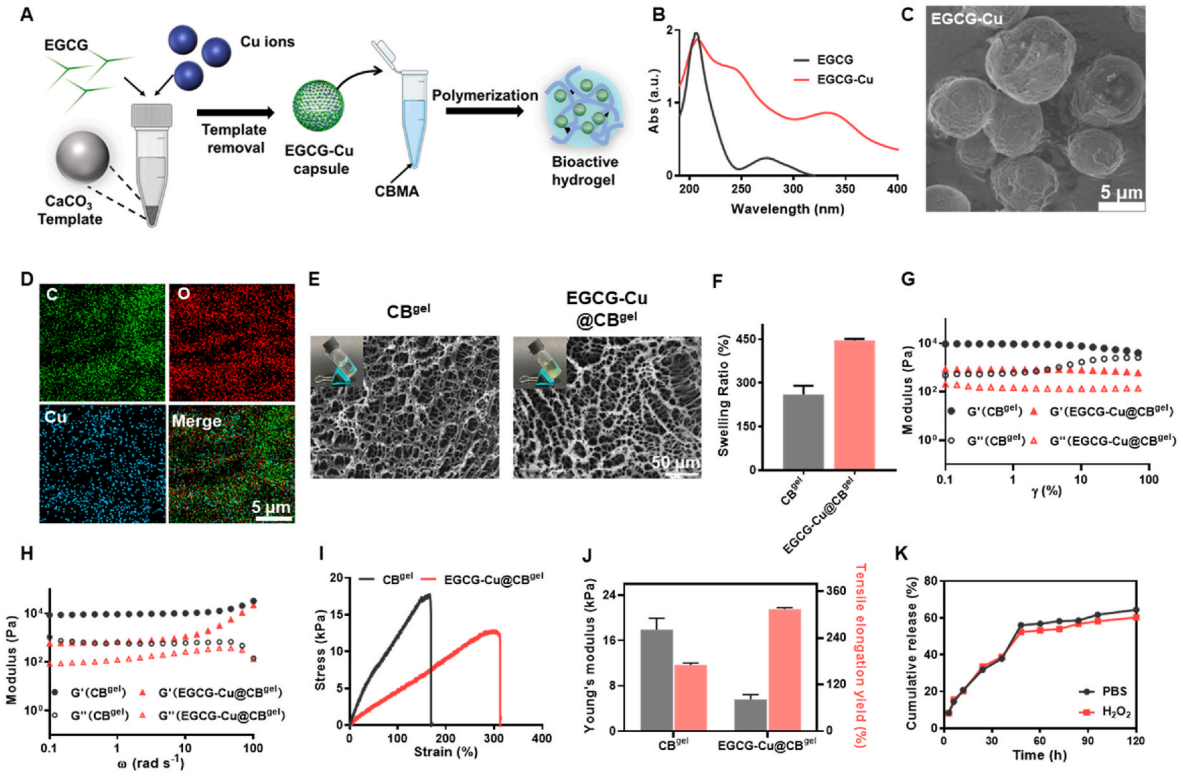

Fig. 2. Synthesis and physicochemical properties of EGCG-Cu@CB^{gel}. (A) Schematic diagram of the synthesis of EGCG-Cu@CB^{gel}. (B) UV–Vis spectra of EGCG and EGCG-Cu capsules. (C) SEM image and (D) EDX elemental mapping of EGCG-Cu capsules. Scale bar is 5 μm. (E) SEM images and (F) swelling ratio of CB^{gel} and EGCG-Cu@CB^{gel}. (G) Rheological analysis of EGCG-Cu@CB^{gel} under strain sweep in the range of 0.1–100%, and (H) frequency sweep in the range of 0.1–100 rad s^{-1} at 25 °C. (I) Tensile stress-strain curves and (J) Young's modulus and tensile elongation of EGCG-Cu@CB^{gel}. (K) *In vitro* release of Cu^{2+} from EGCG-Cu@CB^{gel} in the absence or presence of H_2O_2 (40 mM).

The successful coordination of Cu^{2+} with EGCG was first proven *via* the UV–Vis spectra. A characteristic absorption peak of EGCG at 274 nm gradually decreased after Cu complexation, while a new characteristic absorption peak appeared at 325 nm, due to the formation of specific three-dimensional structure of EGCG combined with Cu^{2+}, leading to red-shift of the maximum absorption of EGCG, demonstrating the successful complexation of Cu with EGCG (Fig. 2B). The peak at 250 nm might be assigned to the typical absorption of a minimal amount of EDTA-Cu chelation compound [44,45]. The presence of Cu^{2+} in EGCG-Cu capsule was confirmed *via* XPS measurements (Figure S1A). After chelation with Cu^{2+}, O1s peak corresponding to the HO–C group splited from 533.1 eV to a new peak at 531.8 eV, indicating electron transfer from Cu^{2+} to EGCG (Figure S1B). Furthermore, SEM revealed that EGCG-Cu capsules exhibited spherical morphology, and Cu^{2+} were uniformly distributed in the capsules (Fig. 2C and D). Additionally, FTIR spectra and surface charges were examined during preparation. The typical EGCG peaks were observed in EGCG-Cu@$CaCO_3$ and EGCG-Cu capsules at 3440 cm^{-1} (Figure S2A). A peak at 876 cm^{-1} was the characteristic vibrational band of vaterite, which disappeared after the removal of $CaCO_3$ template. The surface charge of EGCG-Cu capsule was increased to -14.60 ± 0.26 mV after removing the $CaCO_3$ template (Figure S2B). Furthermore, EDS results (Figure S2C) showed the disappearance of Ca signal in EGCG-Cu capsules, indicating $CaCO_3$ template was completely removed. In addition, Cu^{2+} content in EGCG-Cu capsule was 7.88 wt%, which was measured by ICP-MASS. Therefore, these results confirmed the successful preparation of EGCG-Cu capsules.

To improve EGCG bioavailability and reduce Cu^{2+} toxicity, EGCG-Cu was loaded in hydrogel to retain the bioactive substances at the wound site in a sustainable controlled-release manner. EGCG-Cu@CB^{gel} was prepared by free radical copolymerization of CB monomer and CBOX crosslinking agent. SEM images showed that both CB^{gel} and EGCG-Cu@CB^{gel} possess a uniform three-dimensional network with highly porous structures (Fig. 2E). The strong hydration capacity of zwittrionic moities enabled the hydrogel to rapidly swell in water and held a large volume of water without dissolution. The swelling ratio of EGCG-Cu@CB^{gel} was significantly higher than that of CB^{gel} ($446 \pm 5\%$ *vs* $256 \pm 30\%$) (Fig. 2F). The effect of EGCG-Cu on the mechanical properties of CB^{gel} was investigated *via* rheological analysis. Both G' and G'' of the hydrogel decreased with the addition of EGCG-Cu, and the value of G' was maintained higher than that of G'', indicating that EGCG-Cu@CB^{gel} maintained elastic solid-like property at a strain of 0.1–100% ($\omega = 1$ rad s^{-1}) and angular frequencies of 0.1–100 rad s^{-1} ($\gamma = 1\%$) (Fig. 2G and H). Time-scanning rheological analysis showed that the hydrogels with different concentrations of EGCG-Cu were stable (Figure S3). Beyond that, wound dressings required mechanical flexibility to ensure skin adaptability during tissue movement and deformation. The maximum stress and strain of CB^{gel} were 17.78 kPa and 171%, respectively, while these of EGCG-Cu@CB^{gel} were 12.84 kPa and 314% (Fig. 2I and J). The Young's modulus of CB^{gel} was greater than that of EGCG-Cu@CB^{gel}, while the elongation at break of EGCG-Cu@CB^{gel} was significantly higher than that of CB^{gel} (314.2% *vs.* 170.7%). Thus, the introduction of EGCG-Cu softened the zwitterionic hydrogel and decreased the rigidity and brittleness, thereby improving the adaptability to skin wounds. These results indicated that EGCG-Cu encapsulation did not obviously change the water absorption and rheological properties of CB^{gel}, but improved the tissue adaptability of the hydrogel by promoting the elasticity.

The release kinetics of Cu^{2+} in EGCG-Cu@CB^{gel} were then investigated. As shown in Fig. 2K, when incubated in PBS or H_2O_2 solution, EGCG-Cu@CB^{gel} displayed a sustained release of Cu^{2+} with a similar profile over 120 h, demonstrating the insensitivity of the hydrogel to H_2O_2 and retention of Cu^{2+} in the oxidizing environment. The accumulative release of Cu^{2+} in the first 60 h could reach ~50%, and then plateaued with a total release content of ~60% over 120 h. A sustained release pattern could maintain Cu^{2+} at a low concentration, which might be a feasible approach to avoid unnecessary tissue toxicity [34]. These results confirmed that CB^{gel} encapsulating EGCG-Cu capsules was successfully fabricated with crosslinked network, water retention, flexibility, and prolonged release of Cu^{2+}.

3.2. Cytocompatibility, proliferation, migration, angiogenesis, and antioxidant activities of EGCG-Cu@CB^{gel} in vitro

Cytocompatibility is an essential and prerequisite for biomaterials as wound dressings. The cytotoxicity of EGCG-Cu@CB^{gel} was studied against NIH-3T3 cells *via* live/dead staining (Fig. 3A). Massive red fluorescent cells (dead cells) appeared in $CuCl_2$ group, while more than 95% of NIH-3T3 cells incubated with EGCG-Cu@CB^{gel} survived, as evidenced by numerous green fluorescent cells (alive cells), and almost no red fluorescent cells (dead cells) were observed, indicating that encapsulation of EGCG-Cu capsule in CB^{gel} could prevent the toxicity of high concentration of Cu^{2+}. CCK-8 assay demonstrated the cell viability in $CuCl_2$ group was significantly decreased to 21%, while that of the other groups remained at ~100%, confirming a favorable cytocompatibility of EGCG-Cu@CB^{gel} (Fig. 3B).

Endothelial cell migration is a crucial step in angiogenesis and vascular repair [46]. Consequently, the ability of the bioactive hydrogels to promote cell migration was evaluated. The migration of HUVECs cultured with EGCG-Cu@CB^{gel} extracts was significantly enhanced (Fig. 3C and D). Moreover, as shown in Fig. 3E and F, HUVECs co-cultured with EGCG-Cu@CB^{gel} extracts demonstrated much more junctions and higher tube densities than untreated or CB^{gel}-treated cells, indicating a pro-angiogenesis capability of EGCG-Cu. Interestingly, cell migration and tube formation were also improved in CB^{gel} group compared with control group, possibly due to the ionic conductivity of zwitterionic polymer that could recruit vascular endothelial cells and promote cell migration [47], and the inhibition of methylation reactions and detoxification of homocysteine by the betaine structure in zwitterionic polymers [48]. Then, the expression level of VEGF in HUVECs after treatment with EGCG-Cu@CB^{gel} was measured. EGCG demonstrated no significant influence on the cytotoxicity and expression of VEGF at concentration lower than 25 μg mL^{-1} (Figure S4Aand S4B) [30]. In comparison, EGCG-Cu@CB^{gel} markedly elevated the expression of VEGF in HUVECs (Fig. 3G), which was mainly attributed to the release of Cu^{2+} that could promote the secretion of VEGF [49]. Collectively, these results suggested that EGCG-Cu@CB^{gel} with favorable cytocompatibility could significantly promote cell proliferation, migration, and angiogenesis, which might facilitate the vascularization and endothelialization during wound healing.

Polyphenols including EGCG, are considered to neutralize free radicals such as hydroxyl (HO•), superoxide (O_2•), nitric oxide (NO•), alkoxyl and peroxyl radicals, and nonradicals such as peroxynitrite ($OONO^-$) and hypochlorite (ClO^-) to exert a direct scavenging action against ROS [50]. It was found EGCG-Cu was able to effectively scavenge free radicals and H_2O_2 in a dose-dependent manner (Fig. 3H and I), certifying its antioxidant activity. With the increase of EGCG-Cu concentration, the scavenging efficiency of free radicals was increased gradually. Compared with the control group, the nitrogen radical concentration was decreased to 50%, and the H_2O_2 scavenging rate was ~35% after treatment with EGCG-Cu (200 μg mL^{-1}). In addition, the scavenging ability of intracellular ROS by EGCG-Cu was also investigated, according to the experimental protocol shown in Fig. 3J. First, it was confirmed that EGCG and EGCG-Cu capsules were nontoxic against HUVECs at concentration lower than 50 μg mL^{-1} (Figure S4C). DCFH-DA probe was used to detect intracellular ROS, and Rosup was used as the positive control. After treatment with Rosup, HUVECs showed a strong DCF fluorescence signal, indicating the high levels of intracellular ROS (Fig. 3K). EGCG-Cu treatment significantly reduced the fluorescence signal, suggesting EGCG-Cu could obliterate intracellular ROS. Flow cytometric analysis (Fig. 3L) also showed that the fluorescence intensity (FI) of cells incubated with EGCG-Cu was significantly reduced compared with the positive control. The excessive

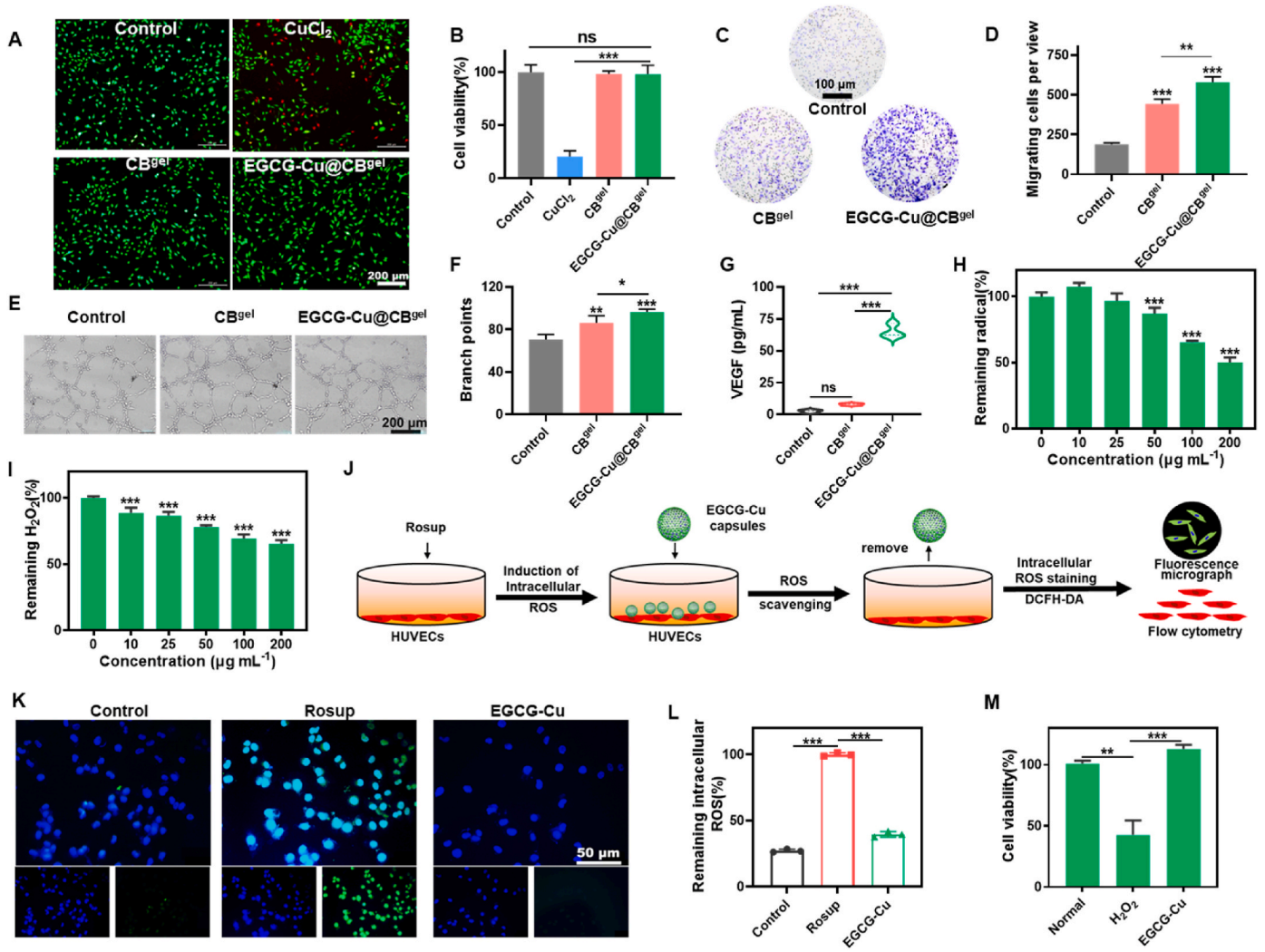

Fig. 3. Cytocompatibility, proliferation, migration, angiogenesis and antioxidant activities of EGCG-Cu@CB^{gel} *in vitro*. (A) Live/dead staining of NIH-3T3 cells after incubation with EGCG-Cu@CB^{gel}. (B) Evaluation of the cytotoxicity against NIH-3T3 cells. (C, D) Representative images and quantitative analysis of the transwell migration assay and (E, F) tube formation for HUVECs. (G) Levels of VEGF in culture supernatants of HUVECs treated with EGCG-Cu@CB^{gel}. (H) Free radical elimination *via* EGCG-Cu capsules. (I) *In vitro* H_2O_2 scavenging ability of EGCG-Cu capsules. (J) Schematic illustration of intracellular ROS scavenging. (K) Representative fluorescence micrographs of Rosup-stimulated HUVECs. (L) Remaining intracellular ROS of Rosup-stimulated HUVECs after incubation with EGCG-Cu capsules. (M) Cell survival rate after H_2O_2 stimulation (Concentration, 25 μg mL^{-1}). ***$p < 0.001$, **$p < 0.01$, *$p < 0.05$; ns, not significant.

intracellular ROS accumulation could disrupt chemical bonds in DNA, lipids and proteins, causing cell apoptosis and necrosis [18]. Subsequently, CCK-8 assay was performed to verify the protective effect on cells against H_2O_2. The cell survival rate (Fig. 3M) was decreased to nearly 50% after the addition of 100 mM H_2O_2, whereas the survival rate was significantly increased to approximately 100% after co-incubation with EGCG-Cu, indicating that EGCG-Cu could protect cells from H_2O_2 damage. These results indicated that EGCG-Cu could scavenge intracellular and extracellular free radicals, protecting cells from damage by oxidative environment.

For severe burn wound care, it is also essential to prevent unnecessary bio-adhesion to avoid damage to the newly formed skin and tissues, as well as relieve the severe pain experienced during the nursing process of the burn wound [51,52]. Therefore, the antifouling properties of EGCG-Cu@CB^{gel} were investigated *via* cell adhesion and protein adsorption experiments. Few cells adhered to CB^{gel} and EGCG-Cu@CB^{gel} surface (Figure S5A); instead, cells adhered and spread on the tissue culture polystyrene plates (TCPs), demonstrating effective anti-adhesion ability of CB^{gel}. Furthermore, the antifouling property against non-specific protein absorption was evaluated. As serum albumin was the major protein in blood, bovine serum albumin (BSA) was used to detect protein adsorption on hydrogels. There was a significant reduction in protein adsorption on CB^{gel} and EGCG-Cu@CB^{gel}, down to approximately 6% and 11%, respectively, compared with that on TCPs (Figure S5B). These data indicated that EGCG-Cu@CB^{gel} could effectively avoid adhesion of proteins and cells, and as a non-adhesive wound dressing, which was expected to significantly reduce the secondary damage to tissue during dressing replacement.

3.3. EGCG-Cu capsules modulate metabolic reprogramming of macrophages and reduce M1 polarization

Metabolic reprogramming of cells is increasingly recognized as a systematic response of cells to environmental and/or genetic alterations that provide important metabolites to influence cell growth, proliferation, and survival as well as related pathophysiological and toxicological processes, and the metabolic state of immune cells can determine immune responses [32,53]. Therefore, regulating immune cell metabolism might be a vital intervention approach for treating inflammation-related diseases. Previous studies indicated that EGCG could interfere with metabolically related enzymes by inhibiting the activity of glutamate dehydrogenase (GDH) in glutamate metabolism, and suppressing the

activity of lactate dehydrogenase (LDH) and key glycolytic enzymes, including HK and pyruvate kinase (PK), to alter glycolytic outcomes [25,31,54]. Here, we hypothesized that metabolic reprogramming might affect metabolite production from pathways involved in macrophage homeostasis. Mitochondria, as the main sites of metabolism, were at the core of cell metabolic network, and thus, we first investigated the effects of EGCG-Cu on the MMP and production of ATP. The decrease of MMP was a landmark in the early stage of apoptosis, which could be rapidly and sensitively detected by JC-1 dye. The preferential aggregation of JC-1 dye (JC-aggregates) in mitochondria would induce the emission of red fluorescence, while monodisperse JC-1 (JC-monomers) in cytoplasm would emit green fluorescence. As shown in Fig. 4A, more JC-monomers with green fluorescence were observed in macrophages treated with carbonyl cyanide 3-chlorophenylhydrazone (CCCP) or LPS. However, an increase in red fluorescence together with a decrease in green fluorescence was found in EGCG-Cu group, indicating that EGCG-Cu could alleviate the decrease in MMP caused by LPS stimulation. Furthermore, flow cytometry analysis showed that following treatment with CCCP and LPS, the population of cells containing JC-aggregates decreased slightly compared with that in control group, while cells containing JC-monomers were significantly elevated, and co-incubation with EGCG-Cu decreased the percentage of cells with JC-monomers to 29.0% (Figure S5). The ratio of green to red fluorescence intensities (Fig. 4B) was significantly decreased in EGCG-Cu group, indicating EGCG-Cu could protect the mitochondria structure and function from oxidative stress-induced damage. Afterward, ATP production in cells cultured with EGCG-Cu was investigated. Decreased ATP levels indicate the dysfunction of mitochondria, which is usually coincided with the reduction of MMP during apoptosis. Fig. 4C showed that ATP production in RAW 264.7 cells incubated with EGCG-Cu after LPS stimulation was restored to a level comparable with that in control group. These results demonstrated that EGCG-Cu could recover the LPS-induced decline in MMP and ATP to normal levels, preventing the destroy of mitochondrion function caused by detrimental oxidative microenvironment.

Furthermore, inflammation activates macrophages to undergo glycolytic metabolic conversion away from OXPHOS. M1-phenotype macrophages exhibit higher glycolytic enzyme activity compared with that in M2-phenotypes [23,31]. Accordingly, the effect of EGCG-Cu on macrophage metabolism was evaluated. Key metabolites altered in glycolytic and TCA cycles and pathways were shown in Fig. 4D. First, the activities of key enzymes related to glycolysis in macrophages were investigated. HK was the first key enzyme in the glycolytic pathway to control the rate of glucose metabolism, catalyzing the conversion of glucose into glucose 6-phosphate (G-6-P) [55,56]. PFK catalyzed the conversion of fructose-6-phosphate (F-6-P) to fructose-1, 6-diphosphate (F-1,6-P), the second phosphorylation reaction of the glycolytic pathway. As the main rate-limiting enzyme and regulatory point in the glycolytic process, the rate of glycolysis is mainly depended on the activity of PFK [57]. HK and PFK activites were significantly decreased in BMDMs treated by EGCG-Cu, compared with those in the LPS-treated

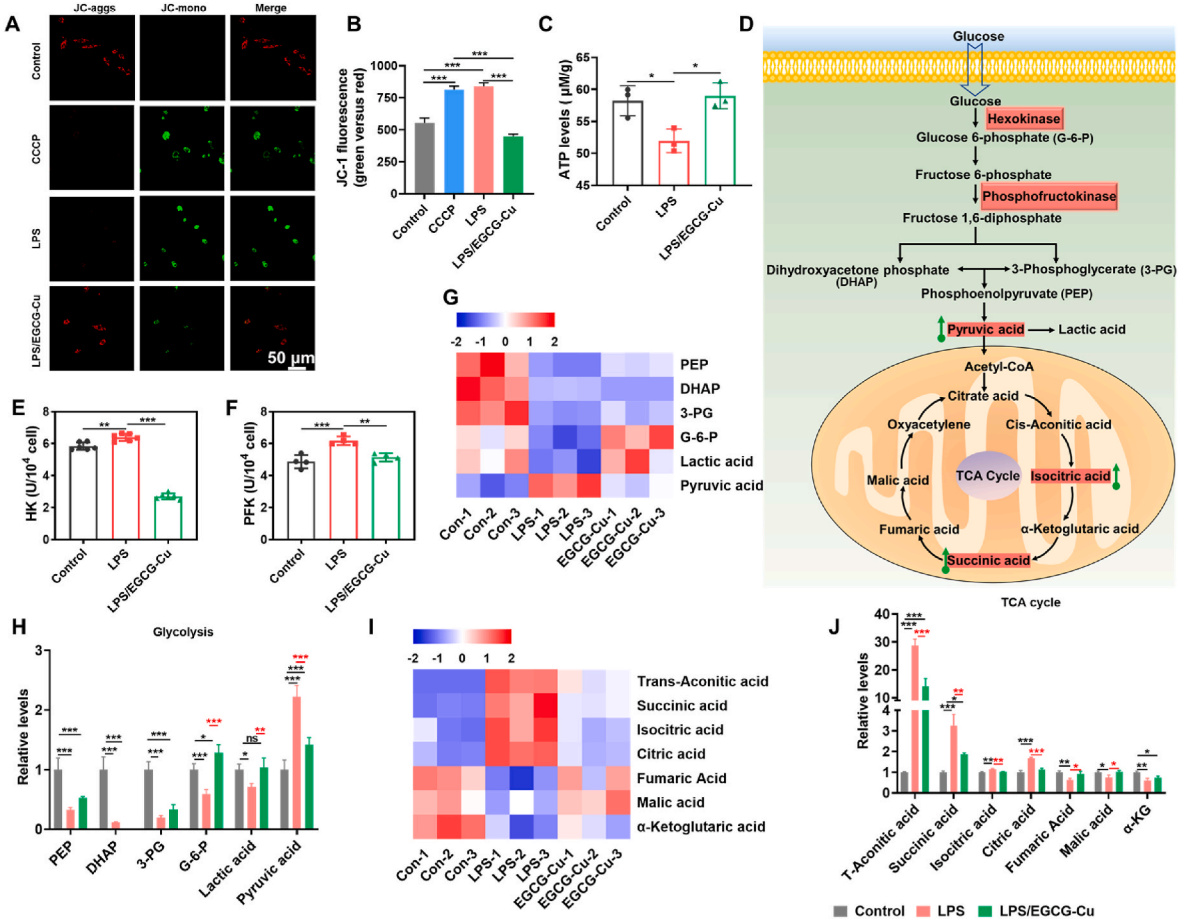

Fig. 4. Metabolic reprogramming by EGCG-Cu. (A) MMPs of macrophages determined *via* JC-1 staining. Red and green fluorescence represents JC-aggregates in healthy mitochondria and cytosolic JC-monomers in compromised mitochondria with collapsed MMPs, respectively. (B) Quantitative analysis of MMPs calculated by the ratios of green to red fluorescence intensity based on flow cytometry (n = 3). (C) Intracellular ATP levels of macrophages (n = 3). (D) Schematic map showing the changes in targeted key metabolites involved in glycolysis and TCA cycle. Enzymatic activity of HK (E) and PFK (F). (G) Heatmap and (H) quantitative analysis of LC-MS data showing the relative abundance of glycolysis metabolites (n = 3). (I) Heatmap and (J) quantitative analysis of the relative abundance of TCA metabolites determined by LC-MS (n = 3). ***$p < 0.001$, **$p < 0.01$, or *$p < 0.05$.

group (Fig. 4E and F). These results suggested that EGCG-Cu could inhibit the activity of key enzymes of glycolysis in an inflammatory state, suppressing the rate and efficiency of glycolytic metabolic in BMDMs.

Cellular metabolism (e.g., glycolysis and TCA) and its related metabolites play a crucial role in the polarization of macrophagepheno type and function. The key metabolites of macrophages co-cultured with EGCG-Cu after LPS stimulation or macrophages incubated in complete medium (control) were analyzed *via* liquid chromatography-tandem mass spectrometry (LC-MS). The heat map (Fig. 4G) and quantitative analysis (Fig. 4H) showed that the levels of key metabolites of glycolysis, including phosphoenolpyruvate, dihydroxyacetone phosphate, 3-phosphoglycerate, and G-6-P, were decreased with LPS stimulation. However, the level of pyruvate was increased in comparison with that in control, but decreased with EGCG-Cu treatment. After glycolysis, pyruvate faces several routes: reduction to lactate catalyzed *via* LDH, simple decarboxylation to ethanol catalyzed *via* pyruvate decarboxylase with the release of carbon dioxide, or oxidized to acetyl coenzyme A (CoA) in mitochondria [58]. The first two routes were commonly adopted in anaerobic environment and the third was chosen in aerobic environment. After LPS treatment, macrophages were in an inflammatory state with a predominantly glycolytic metabolism. Therefore, pyruvate was mainly converted to lactate or ethanol. However, the lactate content in LPS-stimulated macrophages was slightly decreased (Fig. 4H), due to anaerobic metabolic burst with a sharp increase in pyruvate concentration. The intracellular kinetics of lactate might be influenced by the LDH isoenzyme pattern, with LDHA favoring lactate production, which was not inhibited by high pyruvate concentrations; whereas LDHB favored pyruvate production, which was inhibited by high pyruvate concentrations. Thus, LDHA deficiency could elevate pyruvate levels [59,60]. Furthermore, pyruvate accumulation stabilized HIF-1α and induced the expression of HIF-1α regulatory genes, which would further exacerbate inflammation [61]. Pyruvate could be converted to acetyl CoA *via* thiamin pyrophosphate and pyruvate dehydrogenase (PDH). However, under thiamin pyrophosphate-deficient conditions, there was a reduction in PDH activity and expression, which would further inhibit the conversion of pyruvate to acetyl CoA and inhibit the TCA cycle. EGCG-Cu treatment could increase the content of thiamin pyrophosphate and alleviate the accumulation of pyruvate by converting pyruvate to acetyl CoA and promoting the normalization of TCA cycle (Figure S7). These data suggested EGCG-Cu could reduce inflammation by downregulating pyruvate, inhibiting glycolytic metabolism and enhancing TCA cycles.

Then, the influence of EGCG-Cu on TCA cycles was further analyzed. LPS stimulation induced a significant increase in the levels of key metabolites, such as *trans*-aconitate, succinate, isocitric acid, and citric acid in macrophages as shown in heat map (Fig. 4I) and quantitative analysis (Fig. 4J), indicating a disruption in TCA cycle. However, after incubation with EGCG-Cu, the levels of these metabolites were significantly decreased. *Trans*-aconitate, as an isomer of *cis*-aconitate, participated in the competition for *cis*-aconitate production and inhibited the TCA cycle. Additionally, TCA cycle were impaired in M1 macrophages, leading to the accumulation of succinic acid and citric acid. Citric acid was translocated to the cytoplasm to generate NADPH, which promoted the production of the inflammation mediator ROS that could stabilize HIF-1α expression. Increased expression and activation of HIF-1α further enhanced the transcription of glycolytic genes to maintain glycolytic metabolism in M1-type macrophages. Excess succinic acid inhibited the activity of proline hydroxylase, which maintained HIF-1α stability and further deteriorated the inflammatory response [24]. These data suggested that EGCG-Cu could reduce inflammation-evoking succinic and citric acid to decrease the HIF-1α expression, effectively ameliorating the increase in glycolysis and the inhibition of TCA cycle induced by LPS stimulation.

To verify the immunomodulatory effect, BMDMs were stimulated by EGCG-Cu. Cells cultured in normal complete medium and LPS-stimulated cells were used as the negative and positive control group, respectively. Immunofluorescence staining (Fig. 5A) showed that after co-incubation with EGCG-Cu for 24 h, the expression of typical M1 macrophage marker CD80 was significantly decreased in comparison with LPS treatment, and flow cytometry analysis indicated the percentage of M1-type ($F4/80^{+}CD80^{+}$) macrophages was decreased to 6.61% after EGCG-Cu treatment (Fig. 5B and C), confirming that EGCG-Cu could reduce M1 macrophage polarization and relief the inflammatory response induced by LPS. In addition, the expression of inflammation-related genes was detected *via* qRT-PCR (Fig. 5D). EGCG-Cu treatment dampened the pro-inflammatory effect of LPS, as evidenced by the low expression of typical M1-type macrophage-related genes encoding iNOs, IL-1β and CD86. Previous studies had reported that relatively high concentrations of Cu^{2+} ions (above 100 μM) increased the expression of M1-related markers. Nevertheless, releasing Cu^{2+} from biomaterials could induce the M2 phenotype, suggesting that macrophage phenotype could be dependent on the concentration of the ion [62,63]. Moreover, the effect of Cu on macrophage phenotype changes of EGCG was assessed. The results showed that, compared with EGCG, there was no significant change in the effect of EGCG-Cu in decreasing the expression of M1 macrophage marker, indicating that Cu^{2+} of this concentration did not change the modification effect of EGCG on macrophages (Figure S8). Pro-inflammatory cytokines, such as TNF-α and IL-6 secreted by cells in the culture medium supernatant were also assayed. Following co-incubation with EGCG-Cu, the expression of TNF-α and IL-6 by LPS-treated BMDMs (Fig. 5E and F) was significantly decreased from 175 to 102 pg mL^{-1} and from 693 to 427 pg mL^{-1}, respectively. These findings suggested that by effectively reducing macrophage M1 polarization, the expression of inflammatory genes and the secretion of pro-inflammatory cytokines, EGCG-Cu could regulate the inflammatory response.

HIF-1α is a key reprogrammer of inflammatory cell metabolism from OXPHOS to glycolysis [24,26]. Hence, the NF-κB signaling pathway and expression of HIF-1α were evaluated. Fig. 5G showed that EGCG-Cu treatment effectively downregulated NF-κB p65 phosphorylation and HIF-1α expression. Quantitative analysis (Fig. 5H and I) further revealed that the phosphorylation level of NF-κB p65 was decreased by 38.46% after EGCG-Cu treatment, compared with that following LPS treatment (0.40 ± 0.05 *vs.* 0.65 ± 0.05), while HIF-1α was decreased by 28.94% (0.36 ± 0.05 *vs.* 0.51 ± 0.01). These results demonstrated that EGCG-Cu might alleviate inflammation through both HIF-1α and NF-κB signaling pathways, while in-depth mechanism deserved study in future.

3.4. EGCG-Cu@CB^{gel} promotes burn wound healing in vivo

The unique advantages of EGCG-Cu@CB^{gel}, including antioxidantion, cellular metabolism regulation and anti-inflammation were expected to accelerate the healing of burn wounds. The therapeutic strategy was illustrated in Fig. 6A. First, a circular burn wound with a diameter of ~8 mm on the back of mice was obtained using scald apparatus. Representative macroscopic images and wound closure at different time points were presented in Fig. 6B–D. On day 3, EGCG-Cu@CB^{gel} group displayed a smaller wound area than that in other groups. On day 7, compared with control and CB^{gel} groups, the wound area of EGCG-Cu and EGCG-Cu@CB^{gel} groups was significantly reduced at 18.7% and 14.4%, respectively. On day 14, wounds cared by EGCG-Cu and EGCG-Cu@CB^{gel} were almost completely healed, with a closure rate of 94.6% ± 1.9% and 97.5% ± 1.0%, respectively, suggesting a faster wound healing process.

Subsequently, histopathology of wounds during healing was analyzed by hematoxylin-eosin (H&E) and Masson's trichrome staining. On day 3, no epidermis formation was observed in any group, but the wound edge in EGCG-Cu@CB^{gel} group was significantly reduced with higher wound edge contraction in comparison with other groups. On day 7, the scab was shed in each group, and epidermis in EGCG-Cu@CB^{gel} group started to regenerate (Fig. 6E). By day 14, the wound was

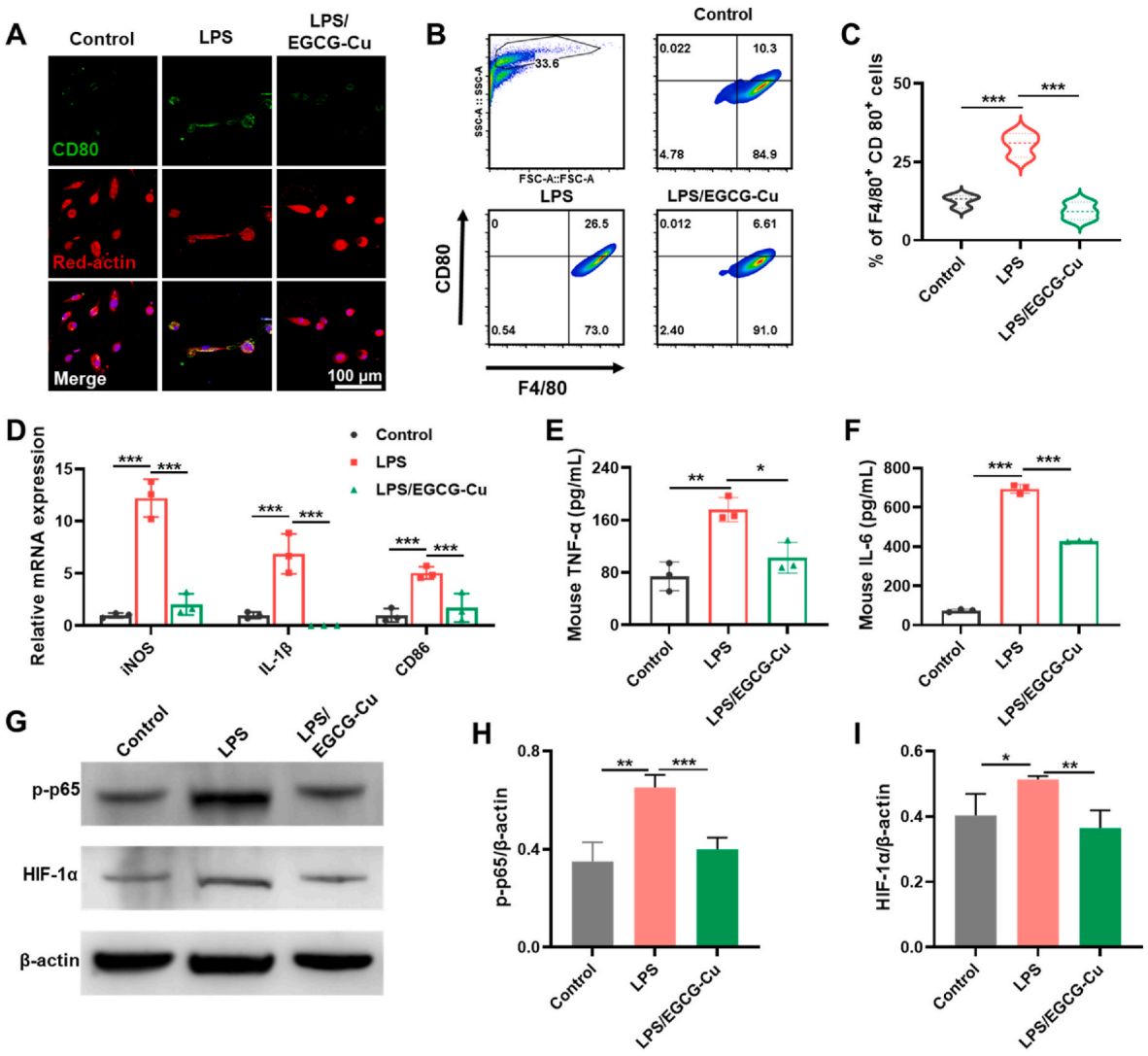

Fig. 5. Regulation of macrophage polarization by EGCG-Cu. (A) Representative CLSM images of BMDMs after treatment with LPS or LPS/EGCG-Cu for 48 h (green, CD80; red, red-actin; blue, cell nuclear). (B) Flow cytometry of CD80 expression (gated on F4/80$^+$ cells). (C) Percentage of M1 type (F4/80$^+$ CD80$^+$) macrophages, n = 3. (D) Relative mRNA expression of iNOs, IL-1β and CD86. (E) Secretion of TNF-α and (F) IL-6 in culture supernatants of macrophages. (G) Protein expression levels of p-p65 and HIF-1α in macrophages determined by western blots. Densitometric analysis of p-p65 (H) and HIF-1α (I). ***$p < 0.001$, **$p < 0.01$, or *$p < 0.05$.

completely closed in each group, and EGCG-Cu@CB^{gel} group displayed the smallest wound edge lengths (red arrows) and the thinnest epidermal thicknesses (Fig. 6F and G). Additionally, more abundant dermal tissue hair follicles (yellow arrows) and neovasculars (red dotted circles) were clearly visible in EGCG-Cu@CB^{gel} group, whereas fewer appendages were regenerated in other groups. These results indicated that EGCG-Cu@CB^{gel} could accelerate burn wound healing, by facilitating the epidermis formation and promoting dermal tissue generation. Collagen, as a major component of the extracellular matrix, plays a critical role in extracellular matrix ECM assembly and tissue reconstruction [64]. Therefore, collagen deposition as a main indicator of remodeling phase during wound healing was assessed *via* Masson's trichrome staining. On day 3, no collagen deposition was observed in any group. By day 7, collagen deposition (blue fibers, Fig. 6H) clearly appeared in EGCG-Cu@CB^{gel} group, whereas there was few collagen deposition in other three groups. EGCG-Cu@CB^{gel} treatment resulted in a significantly higher collagen volume fraction (Figure S9) than the management of CB^{gel} or EGCG-Cu capsule, indicating an accelerated remodeling process. By day 14, compared with the control group, the density of collagen fibers in EGCG-Cu@CB^{gel} group was significantly increased (Fig. 6I), which would promote ECM remodeling. EGCG-Cu@CB^{gel} significantly expedited burn wound healing by boosting epithelialization, dermis maturation, angiogenesis and collagen deposition.

To explore the physiological process of wound repair, immunofluorescence staining was used to evaluate the metabolism of related proteins. First, the antioxidant effect *in vivo* was evaluated by DHE staining. Fig. 7A showed that a large number of red fluorescent cells (DHE$^+$) appeared in the control and CB^{gel} group on day 3, indicating excessive ROS accumulation in the inflammation phase during wound healing. On the contrary, DHE$^+$ cells in EGCG-Cu and EGCG-Cu@CB^{gel} groups were significantly reduced, demonstrating the superior ROS-scavenging effect of EGCG-Cu. The statistical results (Fig. 7D) also showed that EGCG-Cu@CB^{gel} could significantly reduce the level of ROS in the inflammatory phase, compared with the control or EGCG-Cu group, which could relieve the acute inflammation and oxidative stress damage.

Furthermore, angiogenesis was indicated by α-smooth muscle actin (α-SMA) and CD31 staining. The expression of CD31 and α-SMA in EGCG-Cu and EGCG-Cu@CB^{gel} groups was significantly higher than that in other groups (Fig. 7B). More neovasculars and larger vessel diameters were found in EGCG-Cu@CB^{gel} group. Quantitative analysis shown in Fig. 7E and F demonstrated that EGCG-Cu@CB^{gel} induced the highest

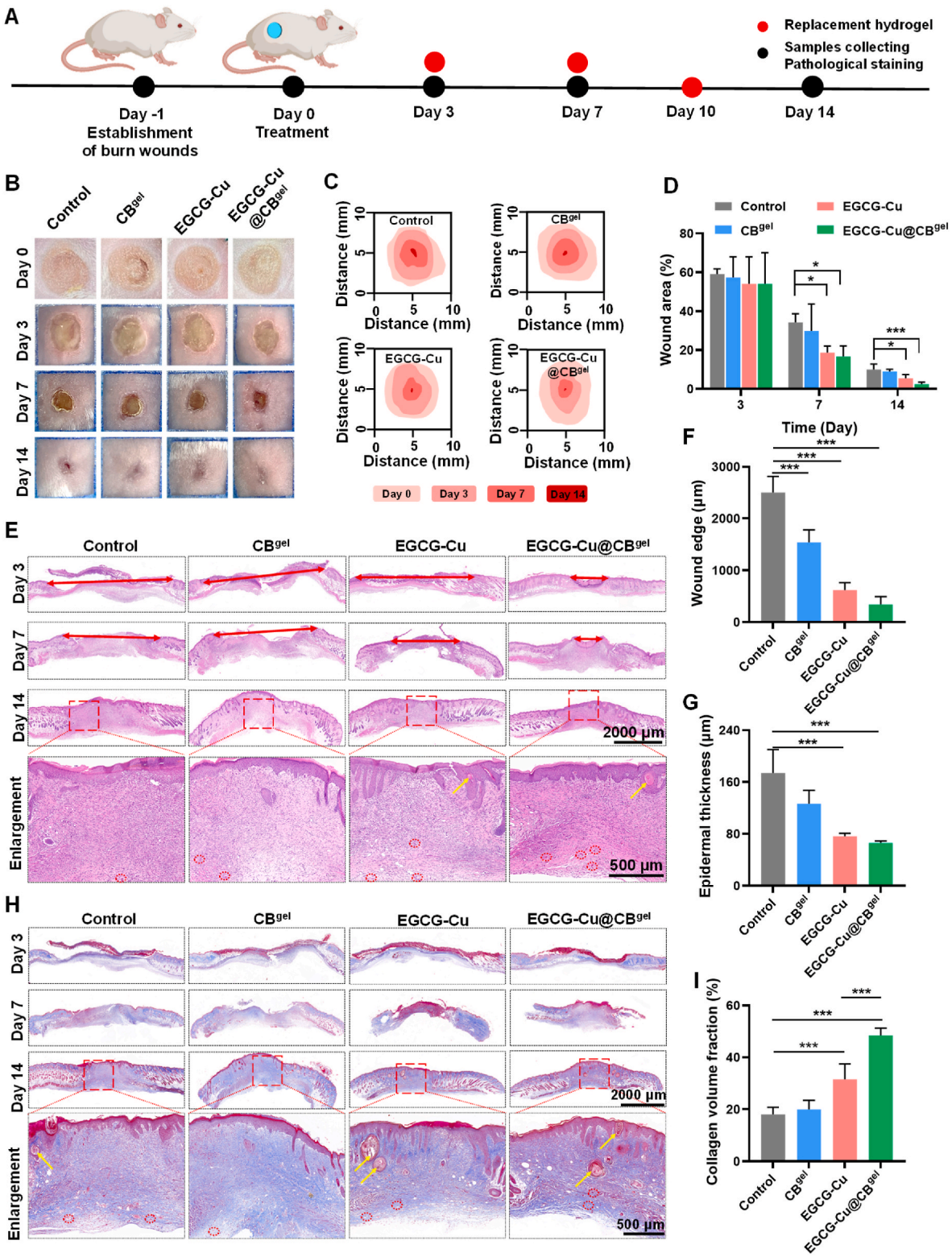

Fig. 6. Burn wound healing accelerated by EGCG-Cu@CB^{gel} in mice. (A) The diagram for burn wound care and experimental procedure. (B) Photographs of treated wounds at day 0, 3, 7, and 14 after surgery. (C) Traces of wound closure. (D) The percentage of wound areas. (E) H&E staining of the wound on day 3, 7, and 14 (red arrows indicate microscopic wound edges, red dotted circles represent blood vessels, yellow arrows indicate granulation tissue). Quantitative analysis of the width of wound edges (F) and epidermal thickness(G) under different treatments on day 14. (H) Masson's trichrome staining of the wound on days 3, 7, and 14 (Red dotted circles represent blood vessels, yellow arrows indicate granulation tissue and collagen deposition is indicated by blue fibers). (I) Quantitative analysis of collagen volume fraction on day 14. Data are shown as mean ± SDs (n = 5). ***$p < 0.001$, and *$p < 0.05$.

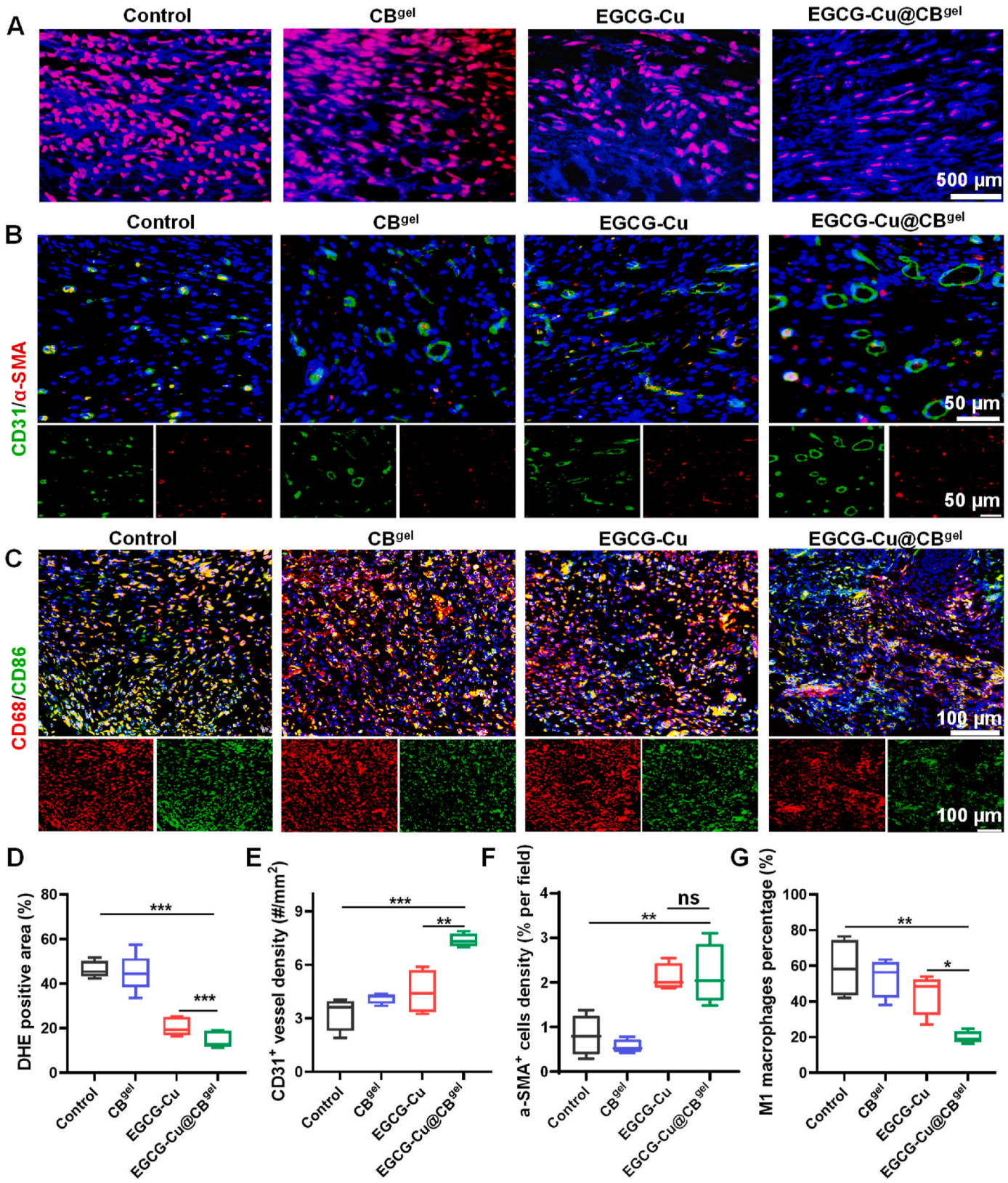

Fig. 7. Immunofluorescence staining of skin tissues post-wounding. (A) The DHE staining on day 3. (B) Representative photographs of CD31 (green) and α-SMA (red) staining on day 14 after wounding. (C) Representative photographs of CD68 (red) and CD86 (green) staining on day 7. (D) Quantitative analysis of DHE staining and the relative expression of CD31 (E) and α-SMA (F), and (G) the percentage of M1 macrophages. Data are shown as mean ± SD (n = 4). ***$p < 0.001$, **$p < 0.01$, or *$p < 0.05$.

expression level of CD31 and α-SMA, which was 2.24- and 2.67-fold higher than those in the control group, respectively, indicating EGCG-Cu sustainably released from CB^{gel} promoted neovascularization during wound healing.

The anti-inflammatory ability of the hydrogel dressing *in vivo* was studied by examining the infiltration and polarization of macrophages in the subcutaneous layer of wounds. Immunofluorescence staining against CD68 marker showed numerous macrophages (red fluorescence) in control and CB^{gel} group (Fig. 7C), indicating a severe inflammatory response after injury. Quantitative data showed that $CD68^{+}CD86^{+}$ M1 macrophages were reduced by 66.25% in the wound tissue treated with EGCG-Cu@CB^{gel} in contrast with that in control group (Fig. 7G), demonstrating sustainable delivery in hydrogel was better than the direct use of EGCG-Cu in dminishing the infiltration of pro-inflammatory M1 macrophages. Thus, EGCG-Cu@CB^{gel} could modulate the local inflammatory response, thereby accelerating the wound healing. Tissue regeneration is an intricate multistep and temporally ordered process that involves a large number of genes, modifiers and pathways. Therefore, further study is needed to determine the exact mechanism by which EGCG-Cu induces wound repair and the application of other trauma models needs to be validated in our next study.

4. Conclusion

In this study, we demonstrated that a bioactive EGCG-Cu@CB^{gel} dressing was successfully developed for severe burn wound care. EGCG-Cu@CB^{gel} showed effective ROS scavenging capability to normalize the intracellular redox homeostasis, and to downregulate M1 type macrophages polarization by modulating the specific glycolysis metabolism, thus inhibiting the inflammatory cycle. Additionally, the sustainable release of Cu^{2+} promoted angiogenesis by inducing higher expression of VEGF. Therefore, by integrating the immunometabolism regulation effect and angiogenesis activity, EGCG-Cu@CB^{gel} significantly accelerated the healing of deep second-degree burn wounds. Altogether, this study confirmed the effectiveness of macrophage metabolic reprogramming in chronic tissue repair. This would allow the development of therapeutic approaches to activate endogenous repair mechanisms, providing great promise in clinical wound care.

Ethics approval and consent to participate

All animal procedures were performed in accordance with the Guidelines for the Care and Use of Laboratory Animals of Peking Union Medical College and experiments were approved by the Animal Experiments and Ethics Review Committee of the Institute of Radiation Medicine, Chinese Academy of Medical Sciences (No. IRM-DWL-2021043).

CRediT authorship contribution statement

Qinghua Li: Writing – original draft. **Huijuan Song:** Methodology. **Shuangyang Li:** Software. **Chuangnian Zhang:** Formal analysis. **Ju Zhang:** Supervision. **Zujian Feng:** Project administration. **Deling Kong:** Conceptualization. **Weiwei Wang:** Funding acquisition. **Pingsheng Huang:** Writing – review & editing.

Declaration of competing interest

The authors declare that they have no known competing financial interests or personal relationships that could have appeared to influence the work reported in this paper.

Acknowledgements

This work was supported by the National Natural Science Foundation of China (No. 82272162, 82001954), Fundamental Research Funds for the Central Universities (3332021067, 2019PT350005), Natural Science Fund for Distinguished Young Scholars of Tianjin (21JCJQJC00020), CAMS Innovation Fund for Medical Sciences (2021-I2M-1–052, 2021-I2M-1–058, 2021-I2M-1–065), and Tianjin Innovation and Promotion Plan Key Innovation Team of Implantable and Interventional Biomedical Materials.

Appendix A. Supplementary data

Supplementary data to this article can be found online at https://doi.org/10.1016/j.bioactmat.2023.07.011.

References

[1] M.G. Jeschke, M.E. van Baar, M.A. Choudhry, K.K. Chung, N.S. Gibran, S. Logsetty, Burn injury, Nat. Rev. Dis. Prim. 6 (2020) 11, https://doi.org/10.1038/s41572-020-0145-5.

[2] Y. Wang, J. Beekman, J. Hew, S. Jackson, A.C. Issler-Fisher, R. Parungao, S. S. Lajevardi, Z. Li, P.K.M. Maitz, Burn injury: challenges and advances in burn wound healing, infection, pain and scarring, Adv. Drug Deliv. Rev. 123 (2018) 3–17, https://doi.org/10.1016/j.addr.2017.09.018.

[3] K. Chen, D. Henn, M. Januszyk, J.A. Barrera, C. Noishiki, C.A. Bonham, M. Griffin, R. Tevlin, T. Carlomagno, T. Shannon, T. Fehlmann, A.A. Trotsyuk, J. Padmanabhan, D. Sivaraj, D.P. Perrault, A.I. Zamaleeva, C.J. Mays, A.H. Greco, S.H. Kwon, M.C. Leeolou, S.L. Huskins, S.R. Steele, K.S. Fischer, H.C. Kussie, S. Mittal, A.M. Mermin-Bunnell, N.M. Diaz Deleon, C. Lavin, A. Keller, M. T. Longaker, G.C. Gurtner, Disrupting mechanotransduction decreases fibrosis and contracture in split-thickness skin grafting, Sci. Transl. Med. 14 (2022), eabj9152, https://doi.org/10.1126/scitranslmed.abj9152.

[4] B.K. Sun, Z. Siprashvili, P.A. Khavari, Advances in skin grafting and treatment of cutaneous wounds, Science 346 (2014) 941–945, https://doi.org/10.1126/science.1253836.

[5] C. Fuchs, L. Pham, Y. Wang, W.A. Farinelli, R.R. Anderson, J. Tam, MagneTEskin-Reconstructing skin by magnetically induced assembly of autologous microtissue cores, Sci. Adv. 7 (2021), eabj0864, https://doi.org/10.1126/sciadv.abj0864.

[6] L. Chen, Z. Li, Y. Zheng, F. Zhou, J. Zhao, Q. Zhai, Z. Zhang, T. Liu, Y. Chen, S. Qi, 3D-printed dermis-specific extracellular matrix mitigates scar contraction via inducing early angiogenesis and macrophage M2 polarization, Bioact. Mater. 10 (2022) 236–246, https://doi.org/10.1016/j.bioactmat.2021.09.008.

[7] L. Zhou, Z. Zeng, S. Liu, T. Min, W. Zhang, X. Bian, H. Du, P. Zhang, Y. Wen, Multifunctional DNA hydrogel enhances stemness of adipose-derived stem cells to activate immune pathways for guidance burn wound regeneration, Adv. Funct. Mater. 32 (2022), 2207466, https://doi.org/10.1002/adfm.202207466.

[8] J. Teoh, A. Mozhi, V. Sunil, S. Tay, J. Fuh, C.-H. Wang, 3D printing personalized, photocrosslinkable hydrogel wound dressings for the treatment of thermal burns, Adv. Funct. Mater. 31 (2021), 2105932, https://doi.org/10.1002/adfm.202105932.

[9] Y. Zhu, J. Zhang, J. Song, J. Yang, Z. Du, W. Zhao, H. Guo, C. Wen, Q. Li, X. Sui, L. Zhang, A multifunctional pro-healing zwitterionic hydrogel for simultaneous optical monitoring of pH and glucose in diabetic wound treatment, Adv. Funct. Mater. 30 (2020), 1905493, https://doi.org/10.1002/adfm.201905493.

[10] X. Zhao, D. Pei, Y. Yang, K. Xu, J. Yu, Y. Zhang, Q. Zhang, G. He, Y. Zhang, A. Li, Y. Cheng, X. Chen, Green tea derivative driven smart hydrogels with desired functions for chronic diabetic wound treatment, Adv. Funct. Mater. 31 (2021), 2009442, https://doi.org/10.1002/adfm.202009442.

[11] Y. Liang, M. Li, Y. Yang, L. Qiao, H. Xu, B. Guo, pH/glucose dual responsive metformin release hydrogel dressings with adhesion and self-healing via dual-dynamic bonding for athletic diabetic foot wound healing, ACS Nano 16 (2022) 3194–3207, https://doi.org/10.1021/acsnano.1c11040.

[12] J. Zhou, W. Liu, X. Zhao, Y. Xian, W. Wu, X. Zhang, N. Zhao, F.-J. Xu, C. Wang, Natural melanin/alginate hydrogels achieve cardiac repair through ROS scavenging and macrophage polarization, Adv. Sci. 8 (2021), 2100505, https://doi.org/10.1002/advs.202100505.

[13] M. Burgess, F. Valdera, D. Varon, E. Kankuri, K. Nuutila, The immune and regenerative response to burn injury, Cells 11 (2022) 3073, https://doi.org/10.3390/cells11193073.

[14] V. Falanga, R.R. Isseroff, A.M. Soulika, M. Romanelli, D. Margolis, S. Kapp, M. Granick, K. Harding, Chronic wounds, Nat. Rev. Dis. Prim. 8 (2022) 50, https://doi.org/10.1038/s41572-022-00377-3.

[15] Z. Lateef, G. Stuart, N. Jones, A. Mercer, S. Fleming, L. Wise, The cutaneous inflammatory response to thermal burn injury in a murine model, Int. J. Mol. Sci. 20 (2019) 538, https://doi.org/10.3390/ijms20030538.

[16] O. Sierawska, P. Małkowska, C. Taskin, R. Hrynkiewicz, P. Mertowska, E. Grywalska, T. Korzeniowski, K. Torres, A. Surowiecka, P. Niedźwiedzka-Rystwej, Innate immune system response to burn damage-focus on cytokine alteration, Int. J. Mol. Sci. 23 (2022) 716, https://doi.org/10.3390/ijms23020716.

[17] S. Kany, J.T. Vollrath, B. Relja, Cytokines in inflammatory disease, Int. J. Mol. Sci. 20 (2019) 6008, https://doi.org/10.3390/ijms20236008.

[18] Y.E. Kim, S.W. Choi, M.K. Kim, T.L. Nguyen, J. Kim, Therapeutic hydrogel patch to treat atopic dermatitis by regulating oxidative stress, Nano Lett. 22 (2022) 2038–2047, https://doi.org/10.1021/acs.nanolett.1c04899.

[19] S.A. Eming, P.J. Murray, E.J. Pearce, Metabolic orchestration of the wound healing response, Cell Metabol. 33 (2021) 1726–1743, https://doi.org/10.1016/j.cmet.2021.07.017.
[20] C. Zhao, J. Chen, R. Zhong, D. Chen, J. Shi, J. Song, Oxidative-species-selective materials for diagnostic and therapeutic applications, Angew. Chem. Int. Ed. 60 (2021) 9804–9827, https://doi.org/10.1002/anie.201915833.
[21] Z. Tu, Y. Zhong, H. Hu, D. Shao, R. Haag, M. Schirner, J. Lee, B. Sullenger, K. W. Leong, Design of therapeutic biomaterials to control inflammation, Nat. Rev. Mater. 7 (2022) 557–574, https://doi.org/10.1038/s41578-022-00426-z.
[22] H.R. Griffiths, D. Gao, C. Pararasa, Redox regulation in metabolic programming and inflammation, Redox Biol. 12 (2017) 50–57, https://doi.org/10.1016/j.redox.2017.01.023.
[23] B. Kelly, L.A.J. O'Neill, Metabolic reprogramming in macrophages and dendritic cells in innate immunity, Cell Res. 25 (2015) 771–784, https://doi.org/10.1038/cr.2015.68.
[24] S.E. Corcoran, L.A.J. O'Neill, HIF1α and metabolic reprogramming in inflammation, J. Clin. Investig. 126 (2016) 3699–3707, https://doi.org/10.1172/JCI84431.
[25] J.C. van der Mijn, D.J. Panka, A.K. Geissler, H. Verheul, J.W. Mier, Novel drugs that target the metabolic reprogramming in renal cell cancer, Cancer Metabol. 4 (2016) 1–18, https://doi.org/10.1186/s40170-016-0154-8.
[26] G.M. Tannahill, A.M. Curtis, J. Adamik, E.M. Palsson-McDermott, A.F. McGettrick, G. Goel, C. Frezza, N.J. Bernard, B. Kelly, N.H. Foley, L. Zheng, A. Gardet, Z. Tong, S.S. Jany, S.C. Corr, M. Haneklaus, B.E. Caffrey, K. Pierce, S. Walmsley, F. C. Beasley, E. Cummins, V. Nizet, M. Whyte, C.T. Taylor, H. Lin, S.L. Masters, E. Gottlieb, V.P. Kelly, C. Clish, P.E. Auron, R.J. Xavier, L.A. O'Neill, Succinate is an inflammatory signal that induces IL-1β through HIF-1α, Nature 496 (2013) 238–242, https://doi.org/10.1038/nature11986.
[27] M. Shi, Z. Wang, L. Huang, J. Dong, X. Zheng, J. Lu, Y. Liang, J. Ye, Utilization of albumin fraction from defatted rice bran to stabilize and deliver (-)-epigallocatechin gallate, Food Chem. 311 (2020), 125894, https://doi.org/10.1016/j.foodchem.2019.125894.
[28] D. Wu, J. Zhou, M.N. Creyer, W. Yim, Z. Chen, P.B. Messersmith, J.V. Jokerst, Phenolic-enabled nanotechnology: versatile particle engineering for biomedicine, Chem. Soc. Rev. 50 (2021) 4432–4483, https://doi.org/10.1039/D0CS00908C.
[29] Q. Wei, L. Ma, W. Zhang, G. Ma, Z. Hu, EGCG-crosslinked carboxymethyl chitosan-based hydrogels with inherent desired functions for full-thickness skin wound healing, J. Mater. Chem. B 10 (2022) 3927–3935, https://doi.org/10.1039/D2TB00074A.
[30] J. Duan, Z. Chen, X. Liang, Y. Chen, H. Li, X. Tian, M. Zhang, X. Wang, H. Sun, D. Kong, Construction and application of therapeutic metal-polyphenol capsule for peripheral artery disease, Biomaterials 255 (2020), 120199, https://doi.org/10.1016/j.biomaterials.2020.120199.
[31] F. Cai, S. Liu, Y. Lei, S. Jin, Z. Guo, D. Zhu, X. Guo, H. Zhao, X. Niu, Y.B. Xi, Z. Wang, G. Chen, Epigallocatechin-3 gallate regulates macrophage subtypes and immunometabolism to ameliorate experimental autoimmune encephalomyelitis, Cell. Immunol. 368 (2021), 104421, https://doi.org/10.1016/j.cellimm.2021.104421.
[32] G. Ye, W. Lu, L. Zhang, H. Gao, X. Liao, X. Zhang, H. Zhang, J. Chen, Q. Huang, Integrated metabolomic and transcriptomic analysis identifies benzo[a]pyrene-induced characteristic metabolic reprogramming during accumulation of lipids and reactive oxygen species in macrophages, Sci. Total Environ. 829 (2022), 154685, https://doi.org/10.1016/j.scitotenv.2022.154685.
[33] S. Kargozar, F. Baino, S. Hamzehlou, R.G. Hill, M. Mozafari, Bioactive glasses: sprouting angiogenesis in tissue engineering, Trends Biotechnol. 36 (2018) 430–444, https://doi.org/10.1016/j.tibtech.2017.12.003.
[34] J. Xiao, S. Chen, J. Yi, H.F. Zhang, G.A. Ameer, A cooperative copper metal–organic framework-hydrogel system improves wound healing in diabetes, Adv. Funct. Mater. 27 (2017), 1604872, https://doi.org/10.1002/adfm.201604872.
[35] Y. Qiao, J. He, W. Chen, Y. Yu, W. Li, Z. Du, T. Xie, Y. Ye, S. Hua, D. Zhong, K. Yao, M. Zhou, Light-activatable synergistic therapy of drug-resistant bacteria-infected cutaneous chronic wounds and nonhealing Keratitis by cupriferous hollow nanoshells, ACS Nano 14 (2020) 3299–3315, https://doi.org/10.1021/acsnano.9b08930.
[36] B. Zhang, R. Yao, C. Hu, M.F. Maitz, H. Wu, K. Liu, L. Yang, R. Luo, Y. Wang, Epigallocatechin gallate mediated sandwich-like coating for mimicking endothelium with sustained therapeutic nitric oxide generation and heparin release, Biomaterials 269 (2021), 120418, https://doi.org/10.1016/j.biomaterials.2020.120418.
[37] C.W.S. Iv, M.A. Evans, L.L.-W. Wang, N. Baugh, S. Iyer, D. Wu, Z. Zhao, A. Pusuluri, A. Ukidve, D.C. Pan, Cellular backpacks for macrophage immunotherapy, Sci. Adv. 6 (2020) eaaz6579, https://doi.org/10.1126/sciadv.aaz6579.
[38] G. Jia, Z. Li, H. Le, Z. Jiang, Y. Sun, H. Liu, F. Chang, Green tea derivative-based hydrogel with ROS-scavenging property for accelerating diabetic wound healing, Mater. Des. 225 (2023), 111452, https://doi.org/10.1016/j.matdes.2022.111452.
[39] K. Li, G. Xiao, J.J. Richardson, B.L. Tardy, H. Ejima, W. Huang, J. Guo, X. Liao, B. Shi, Targeted therapy against metastatic melanoma based on self-assembled metal-phenolic nanocomplexes comprised of green tea catechin, Adv. Sci. 6 (2019), 1801688, https://doi.org/10.1002/advs.201801688.
[40] E. Urso, M. Maffia, Behind the link between copper and angiogenesis: established mechanisms and an overview on the role of vascular copper transport systems, J. Vasc. Res. 52 (2015) 172–196, https://doi.org/10.1159/000438485.
[41] F. Soncin, J.-D. Guitton, T. Cartwright, J. Badet, Interaction of human angiogenin with copper modulates angiogenin binding to endothelial cells, Biochem. Biophys. Res. Commun. 236 (1997) 604–610, https://doi.org/10.1006/bbrc.1997.7018.
[42] J. Badet, F. Soncin, J.D. Guitton, O. Lamare, T. Cartwright, D. Barritault, Specific binding of angiogenin to calf pulmonary artery endothelial cells, Proc. Natl. Acad. Sci. USA 86 (1989) 8427–8431, https://doi.org/10.1073/pnas.86.21.8427.
[43] K. Liu, L. Liu, H. Guo, R. Xu, X. Liang, Y. Chen, H. Li, X. Fu, X. Wang, H. Chen, Y. Li, J. Yang, Redox modulatory Cu(II)-Baicalein microflowers prepared in one step effectively promote therapeutic angiogenesis in diabetic mice, Adv. Healthcare Mater. 12 (2023), 2202010, https://doi.org/10.1002/adhm.202202010.
[44] F. Ju, Y. Hu, Removal of EDTA-chelated copper from aqueous solution by interior microelectrolysis, Sep. Purif. Technol. 78 (2011) 33–41, https://doi.org/10.1016/j.seppur.2011.01.014.
[45] L. Fei, S. Ren, M. Xijun, N. Ali, Z. Jing, J. Yi, M. Bilal, Efficient removal of EDTA-chelated Cu(II) by zero-valent iron and peroxydisulfate: mutual activation process, Sep. Purif. Technol. 279 (2021), 119721, https://doi.org/10.1016/j.seppur.2021.119721.
[46] G. Chiaverina, L. di Blasio, V. Monica, M. Accardo, M. Palmiero, B. Peracino, M. Vara-Messler, A. Puliafito, L. Primo, Dynamic interplay between pericytes and endothelial cells during sprouting angiogenesis, Cells 8 (2019) 1109, https://doi.org/10.3390/cells8091109.
[47] X. Hu, P. Zhang, J. Liu, H. Guan, R. Xie, L. Cai, J. Guo, L. Wang, Y. Tian, X. Qiu, A Self-Association Cross-Linked conductive zwitterionic hydrogel as a myocardial patch for restoring cardiac function, Chem. Eng. J. 446 (2022), 136988, https://doi.org/10.1016/j.cej.2022.136988.
[48] Y. Ishimoto, Y. Hirota-Takahata, E. Kurosawa, J. Chiba, Y. Iwadate, Y. Onozawa, T. Hasegawa, A. Tamura, M. Tanaka, H. Kobayashi, A novel natural product-derived compound, vestaine A_1, exerts both pro-angiogenic and anti-permeability activity via a different pathway from VEGF, Cell. Physiol. Biochem. 39 (2016) 1905–1918, https://doi.org/10.1159/000447888.
[49] C. Wu, Y. Zhou, M. Xu, P. Han, L. Chen, J. Chang, Y. Xiao, Copper-containing mesoporous bioactive glass scaffolds with multifunctional properties of angiogenesis capacity, osteostimulation and antibacterial activity, Biomaterials 34 (2013) 422–433, https://doi.org/10.1016/j.biomaterials.2012.09.066.
[50] J. Zhang, Y. Fu, P. Yang, X. Liu, Y. Li, Z. Gu, ROS scavenging biopolymers for anti-inflammatory diseases: classification and formulation, Adv. Mater. Interfac. 7 (2020), 2000632, https://doi.org/10.1002/admi.202000632.
[51] J. Wu, Z. Xiao, A. Chen, H. He, C. He, X. Shuai, X. Li, S. Chen, Y. Zhang, B. Ren, J. Zheng, J. Xiao, Sulfated zwitterionic poly(sulfobetaine methacrylate) hydrogels promote complete skin regeneration, Acta Biomater. 71 (2018) 293–305, https://doi.org/10.1016/j.actbio.2018.02.034.
[52] Y. Huangfu, S. Li, L. Deng, J. Zhang, P. Huang, Z. Feng, D. Kong, W. Wang, A. Dong, Skin-adaptable, long-lasting moisture, and temperature-tolerant hydrogel dressings for accelerating burn wound healing without secondary damage, ACS Appl. Mater. Interfaces 13 (2021) 59695–59707, https://doi.org/10.1021/acsami.1c18740.
[53] J. Kim, Regulation of immune cell functions by metabolic reprogramming, J. Immunol. 2018 (2018), 8605471, https://doi.org/10.1155/2018/8605471.
[54] W. Hou, S. Lu, H. Zhao, Y. Yu, H. Xu, B. Yu, L. Su, C. Lin, B. Ruan, Propylselen inhibits cancer cell growth by targeting glutamate dehydrogenase at the NADP+ binding site, Biochem. Biophys. Res. Commun. 509 (2019) 262–267, https://doi.org/10.1016/j.bbrc.2018.12.117.
[55] F. Hinrichsen, J. Hamm, M. Westermann, L. Schröder, K. Shima, N. Mishra, A. Walker, N. Sommer, K. Klischies, D. Prasse, J. Zimmermann, S. Kaiser, D. Bordoni, A. Fazio, G. Marinos, G. Laue, S. Imm, V. Tremaroli, M. Basic, R. Häsler, R.A. Schmitz, S. Krautwald, A. Wolf, B. Stecher, P. Schmitt-Kopplin, C. Kaleta, J. Rupp, F. Bäckhed, P. Rosenstiel, F. Sommer, Microbial regulation of hexokinase 2 links mitochondrial metabolism and cell death in colitis, Cell Metabol. 33 (2021) 2355–2366.e2358, https://doi.org/10.1016/j.cmet.2021.11.004.
[56] Y. Liu, R. Xu, H. Gu, E. Zhang, J. Qu, W. Cao, X. Huang, H. Yan, J. He, Z. Cai, Metabolic reprogramming in macrophage responses, Biomarker Res 9 (2021) 1, https://doi.org/10.1186/s40364-020-00251-y.
[57] L.B. Tanner, A.G. Goglia, M.H. Wei, T. Sehgal, L.R. Parsons, J.O. Park, E. White, J. E. Toettcher, J.D. Rabinowitz, Four key steps control glycolytic flux in mammalian cells, Cell Syst 7 (2018) 49–62.e48, https://doi.org/10.1016/j.cels.2018.06.003.
[58] A.J. Rauckhorst, E.B. Taylor, Mitochondrial pyruvate carrier function and cancer metabolism, Curr. Opin. Genet. Dev. 38 (2016) 102–109, https://doi.org/10.1016/j.gde.2016.05.003.
[59] L.R. Gray, S.C. Tompkins, E.B. Taylor, Regulation of pyruvate metabolism and human disease, Cell. Mol. Life Sci. 71 (2014) 2577–2604, https://doi.org/10.1007/s00018-013-1539-2.
[60] D.M. Dawson, T.L. Goodfriend, N.O. Kaplan, N.O. Kaplan, Lactic dehydrogenases: functions of the two types, Science 143 (1964) 929–933, https://doi.org/10.1126/science.143.3609.929.
[61] K. Zera, J. Zastre, Stabilization of the hypoxia-inducible transcription Factor-1 alpha (HIF-1α) in thiamine deficiency is mediated by pyruvate accumulation, Toxicol. Appl. Pharmacol. 355 (2018) 180–188, https://doi.org/10.1016/j.taap.2018.07.004.
[62] R. Lin, C. Deng, X. Li, Y. Liu, M. Zhang, C. Qin, Q. Yao, L. Wang, C. Wu, Copper-incorporated bioactive glass-ceramics inducing anti-inflammatory phenotype and

regeneration of cartilage/bone interface, Theranostics 9 (2019) 6300–6313, https://doi.org/10.7150/thno.36120.
[63] X. Xu, Y. Lu, X. Yang, Z. Du, L. Zhou, S. Li, C. Chen, K. Luo, J. Lin, Copper-modified Ti6Al4 V suppresses inflammatory response and osteoclastogenesis while enhancing extracellular matrix formation for osteoporotic bone regeneration, ACS Biomater. Sci. Eng. 4 (2018) 3364–3373, https://doi.org/10.1021/acsbiomaterials.8b00736.
[64] T.A. Wynn, Common and unique mechanisms regulate fibrosis in various fibroproliferative diseases, J. Clin. Investig. 117 (2007) 524–529, https://doi.org/10.1172/JCI31487.